Perilipin-2 limits remyelination by preventing lipid droplet degradation

Peer-reviewed author version

LOIX, Melanie; WOUTERS, Elien; VANHERLE, Sam; Dehairs, Jonas; McManaman, James L.; KEMPS, Hannelore; SWINNEN , Jo; HAIDAR, Mansour; BOGIE, Jeroen & HENDRIKS, Jerome (2022) Perilipin-2 limits remyelination by preventing lipid droplet degradation. In: Cellular and molecular life sciences (Print), 79 (10) (Art N° 515).

DOI: 10.1007/s00018-022-04547-0
Handle: http://hdl.handle.net/1942/38677

Perilipin-2 limits remyelination by preventing lipid droplet degradation

Melanie Loix[1,2], Elien Wouters[1,2], Sam Vanherle[1,2], Jonas Dehairs[3], James L. McManaman[4], Hannelore Kemps[1,2], Johannes V. Swinnen [3], Mansour Haidar[1,2*], Jeroen F.J. Bogie[1,2*], Jerome J.A. Hendriks[1,2*]

*Authors contributed equally

[1] Department of Immunology and Infection, Biomedical Research Institute, Hasselt University, Diepenbeek, Belgium

[2] University MS Center Hasselt, Pelt, Belgium

[3] Department of Oncology, Laboratory of Lipid Metabolism and Cancer, LKI – Leuven Cancer Institute, KU Leuven - University of Leuven, Leuven, Belgium.

[4] Department of Obstetrics and Gynaecology, School of Medicine, University of Colorado, Denver, United States of America

Corresponding author: jerome.hendriks@uhasselt.be

Keywords: Lipid droplet associated protein, foamy macrophages, lipolysis, lipophagy, inflammation

ABSTRACT

Foamy macrophages and microglia containing lipid droplets (LDs) are a pathological hallmark of demyelinating disorders affecting the central nervous system (CNS). We and others showed that excessive accumulation of intracellular lipids drives these phagocytes towards a more inflammatory phenotype, thereby limiting CNS repair. To date, however, the mechanisms underlying LD biogenesis and breakdown in lipid-engorged phagocytes in the CNS, as well as their impact on foamy phagocyte biology and lesion progression, remain poorly understood. Here, we provide evidence that LD-associated protein perilipin-2 (PLIN2) controls LD metabolism in myelin-containing phagocytes. We show that PLIN2 protects LDs from lipolysis-mediated degradation, thereby impairing intracellular processing of myelin-derived lipids in phagocytes. Accordingly, loss of *Plin2* stimulates LD turnover in foamy phagocytes, driving them towards a less inflammatory phenotype. Importantly, *Plin2*-deficiency markedly improves remyelination in the *ex vivo* brain slice model and in the *in vivo* cuprizone-induced demyelination model. In summary, we identify PLIN2 as a novel therapeutic target to prevent the pathogenic accumulation of LDs in foamy phagocytes and to stimulate remyelination.

INTRODUCTION

Foamy macrophages and microglia engorged with lipid droplets (LDs) are abundantly present in the central nervous system (CNS) of many neurodegenerative disorders, such as multiple sclerosis (MS), stroke, and spinal cord injury. Here, they acquire their foamy morphology mainly through the clearance of myelin, a protective lipid-rich layer wrapped around axons [1]. Ample evidence indicates that ingestion of myelin by phagocytes dynamically shapes their functional phenotype, and, by doing so, markedly affects lesion progression in demyelinating disorders. With respect to the latter, early-stage myelin-containing macrophages and microglia display a protective phenotype, characterized by the release of immunosuppressive and reparative factors [2-4]. In contrast, prolonged intracellular accumulation of myelin-derived lipids skews phagocytes towards a phenotype that suppresses remyelination [5]. We and others demonstrated that disturbances in the breakdown and efflux of myelin-derived lipids underlie this disease-promoting phenotype [5-7]. To date, however, the molecular mechanisms underlying disturbed lipid processing in foamy phagocytes remain poorly understood. Defining these mechanisms is fundamental for our understanding of CNS lesion progression, and for the development of reparative therapies.

Upon internalization by macrophages and microglia, lysosomal processing of myelin results in the generation of free cholesterol and fatty acids, which, in excess, are stored as cholesteryl esters and triacylglycerol in cytoplasmic LDs [8, 9]. By doing so, LDs not only protect foamy macrophages and microglia against lipotoxicity induced by free fatty acids and cholesterol, but also serve as a reservoir of non-toxic esterified cholesterol and triacylglycerol for membrane formation and maintenance, and for lipid efflux [10]. The main surface proteins on LDs belong to the perilipin/ADRP/TIP47 (PAT) family, of which perilipin-2 (PLIN2), also called adipophilin or adipose differentiation-related protein/ADFP, is the most important subtype in cholesterol-loaded macrophages [11, 12]. Interestingly, few studies indicate that PLIN2 is essential for both LD formation and stability, and its absence in a mouse model of atherosclerosis markedly decreases foam cell and lesion formation [13-16]. In line with these findings, overexpression of *Plin2* increases intracellular lipid accumulation and prevents efflux of lipids from lipid-laden macrophages in atherosclerosis [17, 18]. Yet, whether PLIN2 plays a role in the metabolism of LDs in myelin-laden phagocytes, and to what extent PLIN2 controls the functional phenotype of foamy phagocytes in demyelinating lesions remains unclear.

Here, we report that macrophages increase *Plin2* in a peroxisome proliferator-activated receptor gamma- (PPARγ) dependent manner upon myelin internalization. Loss of *Plin2* reduces LD load in

macrophages by enhancing lipolysis-mediated LD turnover. In parallel, *Plin2*-deficiency suppresses the expression of inflammatory mediators in foamy phagocytes. By using cerebellar brain slices cultures and the *in vivo* cuprizone-induced demyelination model, we further show that *Plin2*-deficiency markedly enhances remyelination. Collectively, these findings identify PLIN2 as a novel therapeutic target to promote remyelination.

METHODS

Antibodies

The following antibodies were used: mouse anti-IBA1 (1:100, Santa-Cruz Biotechnology, 1022-5), mouse anti-CD68 (1:100, eBioscience, 14-0688-22), rabbit anti-PLIN2 (1:30, LSBio, LS-C402989), rabbit anti-ADFP (1:500, Abcam, ab52356), rabbit anti-LC3 (1:500, Sigma-Aldrich, L7543; MBL #PM036), rat anti-LAMP1 (1:500, Abcam, ab25245), rat anti-MBP (1:250, Millipore, MAB386), rabbit anti-NF (1:100, Bio-Rad, Ab8135), rabbit anti-iNOS (1:100, Abcam, ab15323), and mouse anti-F4/80 (1:100, Bio-Rad, MCA497G). The used secondary Alexa Fluor antibodies were Alexa488 (1:500, Life Technologies, A21202), Alexa555 (1:500, Life Technologies, A21430), and Alexa647 (1:500, Life Technologies, A21247). BODIPY® 493/503 (2µM, Thermo Fisher Scientific, D3922) was used to stain the LDs.

Animals

Wild-type C57BL/6 mice were purchased from Envigo (Venray, The Netherlands). *Plin2*$^{-/-}$ mice on a C57BL/6 background were kindly provided by prof. dr. McManaman (University of Colorado at Denver, Aurora, USA) [19]. Mice were maintained on a 12h light/dark cycle with free access to water and either a standard chow diet or special formulations as indicated. All studies were conducted in accordance with the institutional guidelines and approved by the Ethical Committee for Animal Experiments of Hasselt University.

Experimental autoimmune encephalomyelitis

Wild-type C57BL/6 females (11 weeks old) were subcutaneously immunized with 200 µg myelin oligodendrocyte glycoprotein (MOG35-55) peptide emulsified in 200µl complete Freund's adjuvant containing 5mg/ml Mycobacterium tuberculosis (EK-2110 kit; Hooke Laboratories, Massachusetts, USA). Directly after immunization and 24h later, mice received an intraperitoneal injection of 100ng pertussis toxin (EK-2110 kit; Hooke Laboratories). Mice were sacrificed on day 14 post immunization. Spinals cords were isolated and snap frozen for real-time quantitative PCR.

Cuprizone

Acute demyelination was induced in wild-type C57BL/6 males (9-11 weeks old) by feeding them ad libitum a diet of 0.3% (w/w) cuprizone (bis(cyclohexanone)oxaldihydrazone, Sigma-Aldrich) mixed in normal chow for 6 weeks. Upon withdrawal of the cuprizone diet, spontaneous remyelination

occurs. Corpus callosum was isolated and snap frozen after demyelination (6 weeks) and during spontaneous remyelination (7 weeks).

Myelin isolation and phagocytosis

Myelin was isolated from the brains of post-mortem C57BL/6 mice (9-11 weeks old) using sucrose density-gradient centrifugation, as previously described [20]. Briefly, after homogenizing the tissue in a 0.32M sucrose-solution, it was layered over a 0.85M sucrose-solution. Following ultracentrifugation (75 000g, 4°C, 30min), the myelin-containing interface was collected, washed in dH2O, and subjected to osmotic disintegration. Next, a second sucrose density-gradient centrifugation was carried out (75 000g, 4°C, 30min) and the collected myelin was dissolved in PBS. The protein concentration was determined using the BCA protein assay kit (Thermo Fisher Scientific, Erembodegem, Belgium). To evaluate the ability and extent of myelin phagocytosis, myelin was fluorescently labeled with 1,1'-dioctadecyl-3,3,3',3'-tetramethylindocarbocyanine perchlorate (DiI, Sigma-Aldrich). Cells were exposed to 50 µg/ml DiI-labeled myelin for 1.5h at 37°C and analyzed for fluorescence intensity by using the FACSCalibur (BD Biosciences).

Monocyte-derived macrophages

This study was approved by the Medical Ethics Committees of Hasselt University and UZ Leuven. After obtaining written informed consent, heparinized peripheral blood was drawn from healthy donors. Peripheral blood mononuclear cells were isolated from whole blood using density gradient centrifugation, as previously described [21]. Next, $CD14^+$ monocytes were enriched by positive selection according to the manufacturer's guidelines (Stemcell Technologies, Grenoble, France). Isolated monocytes were cultured at 2 x 10^6 cells/ml for 7 days in monocyte-derived macrophage (MDM) culture medium (DMEM-high glucose medium (Sigma-Aldrich, Diegem, Belgium)) supplemented with 10% human serum (Sigma-Aldrich), 50U/ml penicillin, 50U/ml streptomycin and, 2mM L-glutamine (Sigma-Aldrich)) at 37°C and 5% CO_2, to obtain monocyte-derived macrophages (MDMs). Following differentiation, MDMs were collected using PBS/EDTA (10mM) and plated at 0.5 x 10^6 cells/ml in MDM culture medium.

Bone marrow-derived macrophages

Bone marrow cells were harvested from wild-type and *Plin2*$^{-/-}$ C57BL/6 female mice (9-11 weeks old) by flushing the femurs and tibias with PBS. Bone marrow-derived macrophages (BMDMs) were obtained by culturing isolated cells for 7 days in BMDM culture medium (RPMI medium supplemented

with 10% fetal calf serum, 25U/ml penicillin, 25U/ml streptomycin, and 15% L929-conditioned medium (LCM)) at 37°C, 5% CO_2. Afterwards, BMDMs were collected using PBS/EDTA (10mM) and plated at 0.5 x 10^6 cells/ml in BMDM culture medium containing 5% LCM.

Macrophage stimulation and pharmacological treatments

To study the involvement of PPARγ in myelin-induced *Plin2* expression, mouse BMDMs and human MDMs were pretreated with the PPARγ antagonist GW9662 (5μM, Sigma-Aldrich) for 30 minutes, followed by incubation with myelin (50 μg/ml) for 24h. *iNos, Tnfa, Il6, Ccl5, Il10,* and *Tgfβ* expression was determined after incubating BMDMs with myelin (50 μg/ml) for 18h, followed by a stimulation with IFNγ and IL1β (100 ng/ml, PeproTech, London, UK) for 6h. TNFα concentration was determined in the supernatant of BMDMS incubated with myelin (50 μg/ml) for 18h, followed by a stimulation with IFNγ and IL1β (100 ng/ml, PeproTech, London, UK) for 18h. LD levels, cholesterol and glycerol concentration, and the cellular lipidome were studied in BMDMs treated with myelin (50 μg/ml) for 24h, followed by the addition of fresh medium for 24h.

Fluorescence microscopy and image analysis

Snap-frozen brain material containing active MS lesions was obtained from the Netherlands Brain Bank (NBB, Amsterdam, Netherlands). 10μM cryostat sections were made of MS lesions and cuprizone tissue using a Leica CM3050 S cryostat (Leica Microsystems). Sections were fixed in ice-cold acetone and 70% ethanol for 10 and 5 min, respectively. Mouse BMDMs were cultured on glass cover slides and fixed in 4% PFA for 15 min. Cerebellar brain slices were fixed in 4% PFA for 15 min. After blocking non-specific staining using Dako protein block (Agilent, California, USA), sections and BMDMs were incubated overnight at 4°C with relevant primary antibodies diluted in PBS. Cerebellar brain slices were stained by incubating with relevant antibodies diluted in blocking buffer (PBS + 1% horse serum + 5% Triton X-100). Nuclei were stained using 4,6'-diamidino-2-phenylindole (DAPI; Invitrogen). Representative images of MS lesions and cuprizone tissue were taken using a Nikon eclipse 80i microscope and NIS Elements BR 3.10 software (Nikon, Tokyo, Japan). MS lesions, BMDMs, and cerebellar brain slices were imaged using LSM 880 Confocal microscope (Zeiss) using the Airyscan feature. Image J version 1.52c was used for quantification. Three-dimensional analysis of cerebellar brain slices was performed using the z-stack function on the confocal microscope and images were rendered by the 3D rendering software vaa3d [58]. Pictures indicated in figures are digitally enhanced.

RNA extraction and real-time quantitative PCR

Total RNA from cells and tissue was isolated using Qiazol (Qiagen, Venlo, The Netherlands) and the RNeasy mini kit (Qiagen), according to the manufacturer's guidelines. Complementary DNA was synthesized using qScript™ cDNA SuperMix (Quanta Biosciences, VWR, Leuven, Belgium) according to the manufacturer's instructions. Real-time quantitative PCR was conducted on a Step One Plus detection system (Applied biosystems, California, USA). Cycle conditions were 95°C for 20s, followed by 40 cycles of 95°C for 3s, and 60°C for 30s. The PCR reaction mixture contained SYBR green master mix (Thermo Fisher Scientific), 0.3 µM forward and reverse primer (IDT technologies, Leuven, Belgium), RNase free water and 12.5 ng cDNA template. Data were analyzed using the comparative Ct method and normalized to the most stable reference genes, which were determined as previously described [13].

Oil red O staining and quantification

PFA fixed cells and cerebellar brain slices, and unfixed cryosections, were stained with 0.3% Oil Red O (ORO, Merck 1320-06-5) for 10 min. Counterstaining of cell nuclei was done using haematoxylin incubation. Analysis was carried out using a Leica DM 2000 LED microscope and ImageJ software. For ORO quantification in cells, ORO was extracted by incubating the cells with isopropanol for 10 min, while shaking. Absorbance was measured using a microplate reader (BIORAD iMarkTM Microplate Reader, Temse, Belgium) at 510 nm.

Cholesterol measurement

Total and free cholesterol was measured in cell lysates and supernatant using the Amplex™ Red Cholesterol Assay Kit (Thermo Fisher Scientific), according to the manufacturer's instructions. Cholesteryl ester concentration was calculated by subtracting free cholesterol concentration from total cholesterol concentration. To measure cholesterol efflux, cells were exposed to apoA-I (50 µg/ml) or high-density lipoprotein (HDL, 50 µg/ml) in phenol- and serum-free medium for 4h prior to measuring intracellular and extracellular total cholesterol. Cholesterol efflux was determined by dividing fluorescence in the supernatants by the total fluorescence in supernatants and cells. Fluorescence was measured at an excitation wavelength of 540 nm and an emission wavelength of 590 nm using the FLUOstar optima microplate reader (BMG Labtech, Ortenberg, Germany).

LC-ESI-MS/MS

BMDM cell pellets were diluted in 700 µl 1x PBS with 800 µl 1 N HCl:CH3OH 1:8 (v/v), 900 µl $ChCl_3$ and 200 µg/ml of the antioxidant 2,6-di-tert-butyl-4-methylphenol (BHT; Sigma-Aldrich). 3 µl of SPLASH LIPIDOMIX Mass Spec Standard (Avanti Polar Lipids) was added into the extract mix. The organic fraction was evaporated at room temperature using the Savant Speedvac spd111v (Thermo Fisher Scientific), and the remaining lipid pellet was reconstituted in 100% ethanol. Lipid species were analyzed by liquid chromatography electrospray ionization tandem mass spectrometry (LC-ESI-MS/MS) on a Nexera X2 UHPLC system (Shimadzu) coupled with hybrid triple quadrupole/linear ion trap mass spectrometer (6500+ QTRAP system; AB SCIEX). Chromatographic separation was performed on a XBridge amide column (150 mm x 4.6 mm, 3x5 µm; Waters) maintained at 35°C using mobile phase A [1 mM ammonium acetate in water-acetonitrile 5:95 (v/v)] and mobile phase B [1 mM ammonium acetate in water-acetonitrile 50:50 (v/v)] in the following gradient: (0-6 min: 0% B → 6% B; 6-10 min: 6% B → 25% B; 10-11 min: 25% B → 98% B; 11-13 min: 98% B → 100% B; 13-19 min: 100% B; 19-24 min: 0% B) at a flow rate of 0.7 ml/min which was increased to 1.5 ml/min from 13 minutes onwards. SM, CE, CER, DCER, HCEER, LCER were measured in positive ion mode with a precursor scan of 184.1, 369.4., 264.4, 266.4, 264.4, and 264.4. TAG, DAG, and MAG were measured in positive ion mode with a neutral loss scan for one of the fatty acyl moieties. PC, LPC, PE, LPE, PG, PI, and PS were measured in negative ion mode by fatty acyl fragment ions. Lipid quantification was performed by scheduled multiple reactions monitoring (MRM), the transitions being based on the neutral losses or the typical product ions as described above. The instrument parameters were as follows: Curtain Gas = 35 psi; Collision Gas = 8 a.u. (medium); IonSpray Voltage = 5500 V and -4500 V; Temperature = 550 °C; Ion Source Gas 1 = 50 psi; Ion Source Gas 2 = 60 psi; Declustering Potential = 60 V and -80 V; Entrance Potential = 10 V and -10 V; Collision Cell Exit Potential = 15 V and -15 V. Peak integration was performed with the Multiquant TM software version 3.0.3. Lipid species signals were corrected for isotopic contributions (calculated with Python Molmass 2019.1.1) and were quantified based on internal standard signals and adhere to the guidelines of the Lipidomics Standards Initiative (LSI; level 2 type quantification as defined by the LSI). Only the detectable lipid classes and fatty acyl moieties are reported in this manuscript.

Cell viability

To assess cellular viability, cells were incubated with 7AAD (Thermo Fisher Scientific). The FACSCalibur was used to quantify cellular fluorescence. Mean fluorescence intensity (MFI) was corrected for background MFI.

ELISA

TNFα concentration was determined in the supernatant of BMDM cultures using the TNFα mouse ELISA kit, according to the manufacturer's guidelines (88-7324-22, Thermo Fisher Scientific).

NO determination

BMDMs seeded in a 48 well plate were treated with myelin followed by 18 hrs of LPS stimulation as described above. Afterwards, the cell culture supernatants were collected and mixed with the Griess reagent (Sigma Aldrich) at a 1:1 ratio. After 15 minutes incubation at room temperature, the absorbance was measured at 540 nm using the FLUOstar optima microplate reader (BMG Labtech).

Western blotting

Cells were lysed in RIPA buffer (150 mM NaCl VWR, 27810.295], 50 mM Tris (Thermo Fisher Scientific, BD152-5), 1% SDS (Sigma-Aldrich, 75746), 1% Triton X-100, 0.5% sodium deoxycholate (Sigma-Aldrich, 302-95-4), pH 8) supplemented with protease (Roche, 05892970001) -phosphatase (Roche, 04906837001) inhibitor cocktail. Samples were separated by electrophoresis on a 12% gel and were transferred onto a PVDF membrane. Blots were blocked in 5% milk in PBST (137 mM NaCl [VWR, 27810.295], 2.7 mM KCl (VWR, 26764.298, 10 mM Na_2HPO_4 (VWR, 102495), 1.8 KH_2PO_4 (VWR, 26936.293), 0.5% Tween-20 (Thermo Fisher Scientific, BP337), pH 7.2) and were incubated with relevant primary antibodies, followed by incubation with the appropriate HRP-conjugated secondary antibody. An enhanced chemiluminescence (ECL) Plus detection kit (Thermo Fisher Scientific, 32132) was used for detection. Densitometry analysis was performed using ImageJ and normalized to actin.

Glycerol assay

Glycerol levels in BMDMs and brain slice medium were determined using the glycerol assay kit, according to the manufacturer's guidelines (MAK117, Sigma-Aldrich).

Cerebellar slice cultures

Cerebellar slices were obtained from wild-type and *Plin2*$^{-/-}$ C57BL/6 P9 or P10 mouse pups, as described previously [61,62]. Demyelination was induced by treating the slices with lysolecithin (0.5 mg/ml; Sigma-Aldrich) for 16h. For microglia depletion, slices were treated with clodronate or empty liposomes (0.5 mg/ml, LIPOSOMA) immediately after isolation for 24h. After three days, slices were treated with LPC for 16h. Afterwards, slices were washed and kept in culture (MEM supplemented with 25% horse serum, 10% HBSS, 1% P/S, 1.5% glucose, 1% Glutamax and 1.2% 1M HEPES) for 1 week, followed by histological and biochemical analysis.

OPC isolation and culturing

OPCs were isolated from pooled P0-P2 C57BL/6JOlaHsd neonatal mice cerebral cortices. Cortices were isolated, meninges removed, minced and dissociated for 20 min at 37°C with papain and DNase I (both 20 µg/mL, Sigma-Aldrich). The resulting mixed glial cultures were seeded in poly-L-lysine (PLL, 50 µg/ml, Sigma-Aldrich)-coated T75 flasks and cultured (37°C, 8.5% CO_2) in DMEM6429 (Sigma-Aldrich) supplemented with 10% FCS and 1% P/S. After 7 days, the medium was supplemented with insulin (5 µg/ml, Sigma-Aldrich). Medium changes were performed on day 4, 7, 11 and 14. Mixed glial cultures were separated after 14 days by mechanical shaking at 75 rpm for 45min at 37°C (to remove microglia) followed by additional 18h shaking at 250 rpm at 37°C. Medium containing the detached cells was then transferred to petri dishes to further remove microglia and astrocytes based on differential adhesion characteristics (20 min, 37°C, 8.5% CO_2). Afterwards, the enriched OPCs were collected and plated in PLL-coated wells. OPCs were cultured in sato medium (DMEM, 100 µg/ml apo-transferrin, 16 µg/ml Putrescine, 5 µg/ml insulin, 60 ng/ml progesterone, 40 ng/ml sodium selenite, 30 ng/ml triiodothyronine, 40 ng/ml L-Thyroxine, 1% P/S, 2% horse serum, 2% B-27; all from Sigma-Aldrich) supplemented with PDGF and bFGF (both 10 ug/ml, Peprotech) for the first two days to reset their cell cycle. Afterwards, OPCs were cultured in normal sato medium and medium was changed every two days.

Statistics

All data are reported as mean ± standard error of the mean (SEM). Data were statistically analyzed using GraphPad Prism v6 (GraphPad Software, La Jolla, CA, USA). Normal distribution was tested using the D'Agostino-Pearson omnibus normality test. Normally distributed data sets were analyzed using an analysis of variances (ANOVA) or two-tailed unpaired student T-test. Data sets that were

not normally distributed were analyzed using the Kruskal-Wallis or Mann-Whitney analysis. *$P \leq 0.05$, **$P \leq 0.01$, ***$P \leq 0.001$, and ****$P \leq 0.0001$.

RESULTS

Myelin uptake increases PLIN2 expression in macrophages in a PPARγ-dependent manner

Demyelinating lesions are characterized by the abundant presence of foamy macrophages loaded with cholesterol-containing LDs [1]. As PLIN2 is the main LD-associated protein on cholesterol-containing LDs and given its key role in LD biology [22], we first determined PLIN2 distribution in demyelinating lesions. For this purpose, active demyelinating MS lesions were stained for PLIN2 and the macrophage/microglia marker IBA1 and CD68. Lesional macrophages and microglia, containing ample intracellular myelin remnants, showed increased PLIN2 abundance as compared to phagocytes in the normal-appearing white matter (NAWM) surrounding the lesion (Fig. 1A-C, Fig. S1). By using the cuprizone model and experimental encephalomyelitis (EAE) model, which are respectively models for demyelination and neuroinflammation, and are characterized by the abundant presence of foamy phagocytes [5, 23], we further showed increased *Plin2* mRNA expression in the brain and spinal cord of these animals (Fig. 1D,E). Consistent with these findings, human monocyte-derived macrophages (MDMs) and mouse bone marrow-derived macrophages (BMDMs) displayed increased *Plin2* expression following myelin exposure (Fig. 1F,G), which was validated on protein level (Fig. 1H,I).

Previous studies defined that the nuclear receptor PPARγ, which is highly active in myelin-containing macrophages and microglia [4, 24], transcriptionally controls *Plin2* expression [25-27]. To determine whether PPARγ regulates *Plin2* expression in myelin-containing macrophages, MDMs and BMDMs were exposed to myelin and the PPARγ antagonist GW9662. We observed that antagonism of PPARγ counteracted the myelin-induced increase in *Plin2* expression (Fig. 1F,G). Taken together, these data show that PLIN2 levels are increased in foamy phagocytes in actively demyelinating lesions in rodents and humans, and that its expression is regulated by PPARγ.

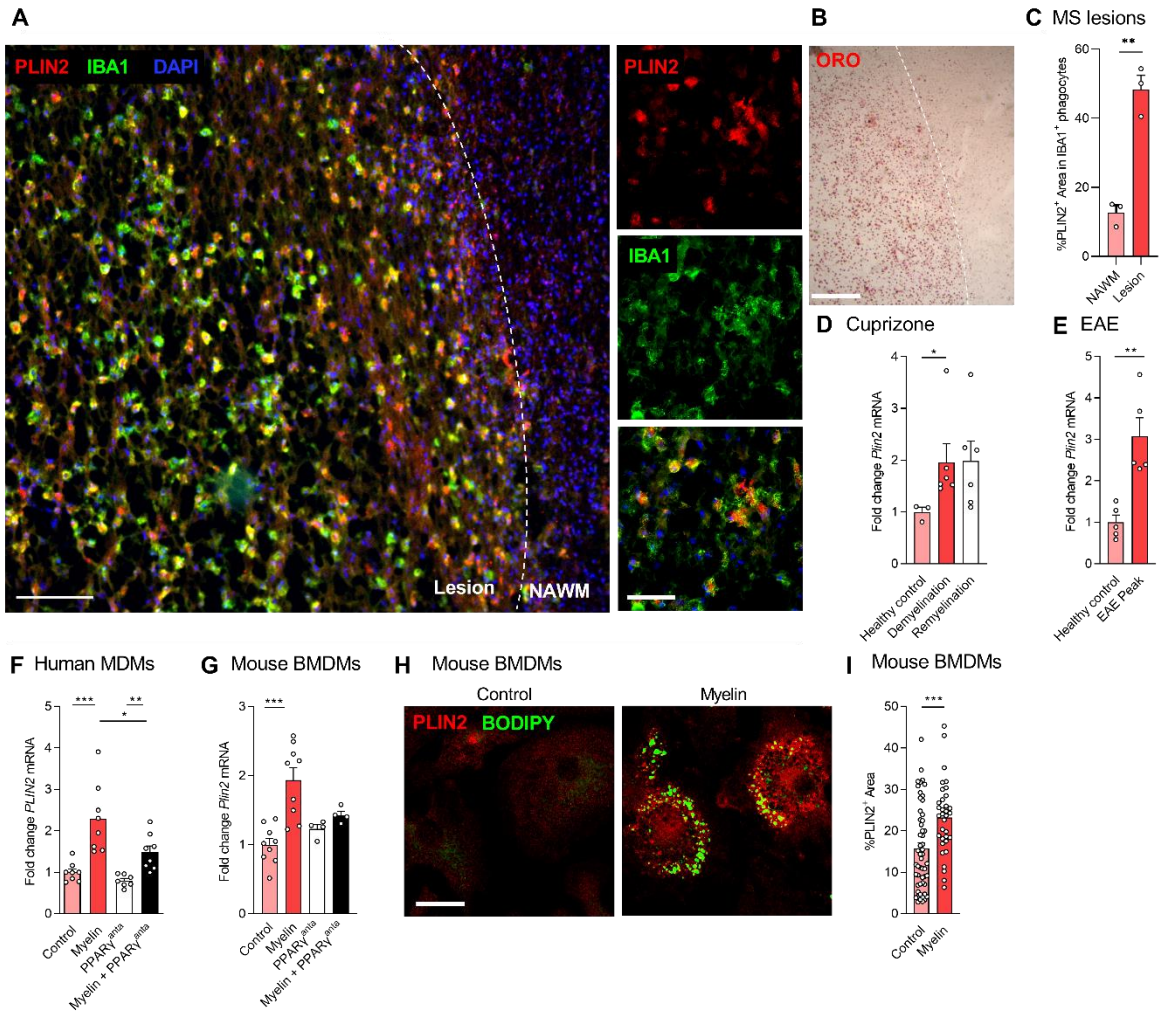

Figure 1. Myelin internalization increases PLIN2 in phagocytes in a PPARγ-dependent manner. A) Representative image of active demyelinating multiple sclerosis (MS) lesion stained for PLIN2 (red) and IBA1 (green) (n=3 lesions from 3 different MS patients). Nuclei were stained using DAPI (blue). Scale bars: 200µm, 50µm. **B)** Representative image of oil red O staining of an active MS lesion. Scale bar: 300µm. **C)** Quantitative analysis of the %PLIN2$^+$ area in IBA1$^+$ phagocytes in normal-appearing white matter (NAWM) and active demyelinating lesions (n=3 lesions from 3 different MS patients). **D)** *Plin2* mRNA in healthy animals, animals sacrificed after 6 weeks of cuprizone diet (demyelination), and animals sacrificed after 6 weeks of cuprizone diet plus one week of normal chow (remyelination) (n=3-6 mice). **E)** *Plin2* mRNA in spinal cord tissue of healthy and experimental autoimmune encephalitis (EAE) animals sacrificed at the peak stage of the disease (n=5 mice). **F,G)** *PLIN2* mRNA in human monocyte-derived macrophages (MDMs, n=8 wells) and murine bone marrow-derived macrophages (BMDMs, n=5 wells) pre-incubated with the PPARγ antagonist (GW9662, 5 µM) followed by myelin treatment (50µg/ml) for 24h (n=4-8 wells). **H,I)** Representative images (H) and quantification (I) of BMDMs treated with myelin (50µg/ml) for 24h and stained for PLIN2 (red) and BODIPY (green). Scale bar: 10µm. (n= >35 cells, data pooled from 3 experiments). Data are represented as mean ± SEM. *P ≤ 0.05, **P ≤ 0.01 and ***P ≤ 0.001.

Plin2-deficient macrophages show an increased rate of LD degradation and lipid efflux

PLIN2 is a member of the PAT family involved in the biogenesis of LDs in multiple cell types such as hepatocytes and fibroblasts [14, 28-30]. However, few studies indicate that PLIN2-deficiency enhances LD breakdown and lipid efflux as well [16, 18]. To assess the role of PLIN2 in LD formation and degradation in myelin-laden macrophages, wild-type and *Plin2*$^{-/-}$ BMDMs were treated with myelin for 24h (LD formation), followed by 24h of myelin-free medium (LD degradation) (Fig. 2A). Neutral lipid-containing structures, which are predominantly present in LDs, were visualized and quantified using the neutral lipid stains Oil Red O (ORO) (Fig. 2B,D) and BODIPY (Fig 2C,E). Upon myelin exposure, wild-type and *Plin2*$^{-/-}$ BMDMs accumulated comparable amounts of ORO^{+} and BODIPY^{+} LDs. Similar findings were obtained after shorter incubation periods with myelin (Fig. S2A,C). In contrast, *Plin2*$^{-/-}$ foamy macrophages showed a reduced LD load following culture in myelin-free medium as compared to wild-type foamy macrophages (Fig. 2B-F, and Fig. S2B). These findings indicate that PLIN2-deficiency promotes the breakdown but does not influence biogenesis of LDs in myelin-containing macrophages. Accordingly, *Plin2*$^{-/-}$ myelin-containing macrophages showed reduced cholesterol ester and increased free cholesterol levels, suggesting enhanced hydrolysis of neutral lipids in LDs (Fig. 2G,H). To assess differences in the complete cellular lipidome of wild-type and *Plin2*$^{-/-}$ macrophages, liquid chromatography electrospray ionization tandem mass spectrometry (LC-ESI-MS/MS) was performed. Similar to our previous findings, there was an overall reduction in the presence of lipid species in *Plin2*$^{-/-}$ macrophages, including but not limited to cholesterol esters and triglycerides, which are the main components of myelin-derived LDs. Importantly, this reduction was more pronounced during the LD degradation phase, further confirming that loss of PLIN2 mainly affects LD load by increasing LD turnover (Fig. 2I,J, and Fig. S3).

Degradation of cholesterol-rich LDs and subsequent release of free cholesterol is essential for ATP-binding cassette A1- and G1- (ABCA1 and ABCG1) mediated lipid efflux. Here, we show that *Plin2*-deficiency increased ABCA1-mediated cholesterol efflux to ApoA1 without affecting ABCG1-mediated efflux to HDL (Fig. 2K). The expression of *Abca1* and *Abcg1* remained unchanged (Fig. S2D). Of note, loss of *Plin2* did not impact myelin uptake or cell viability (Fig. 2L, Fig. S2E, Fig. S2F), nor did it affect the expression of the scavenger receptors *Sra1* and *Cd36* (Fig. S2G) or that of sterol O-acyl transferases *Soat1* and *2* (Fig. S2H). In summary, these findings show that *Plin2*-deficiency boosts LD breakdown and consequent lipid efflux in myelin-laden macrophages.

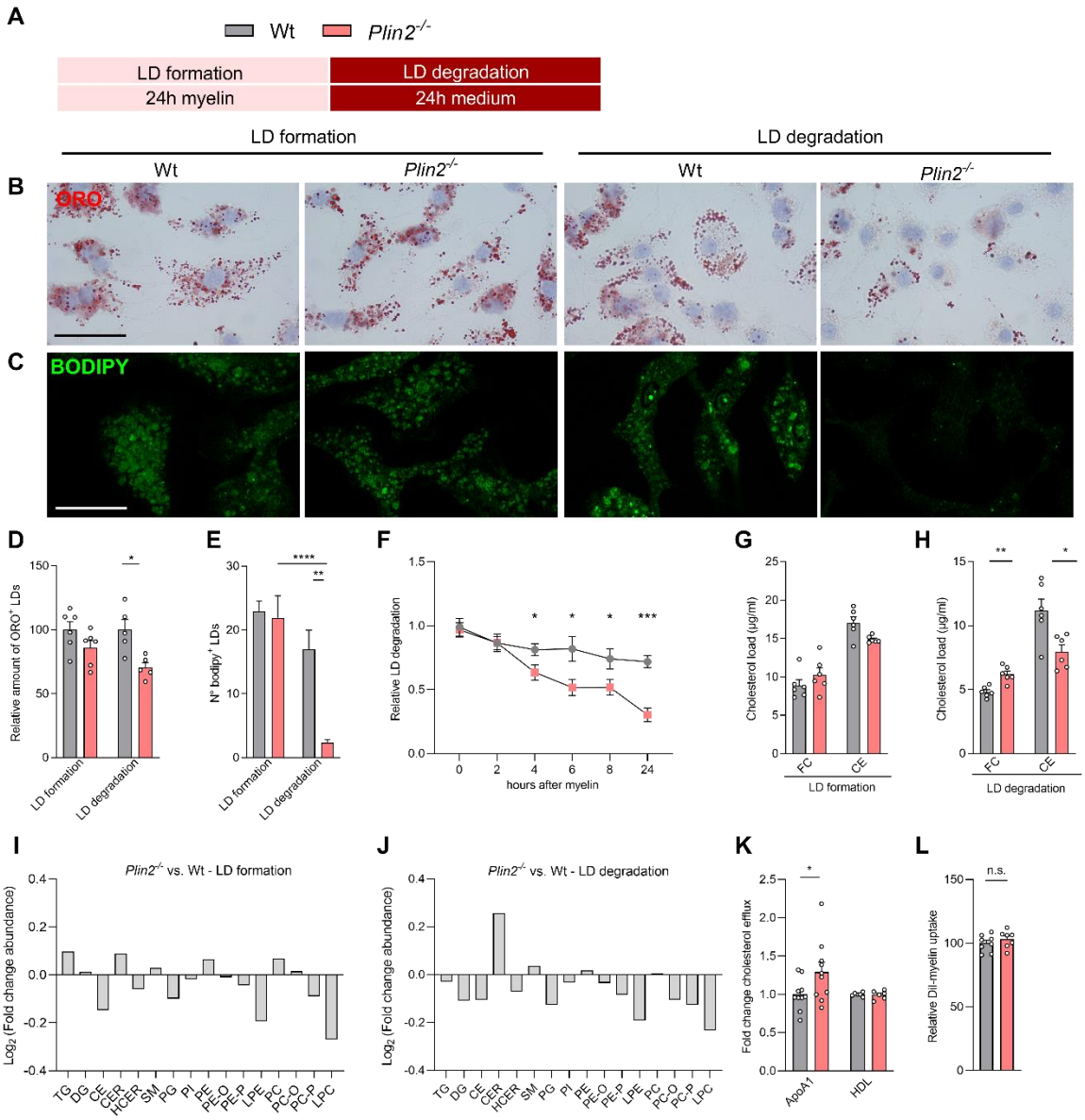

Figure 2. Increased LD degradation and lipid efflux in *Plin2*-deficient foamy macrophages. A) Schematic overview of the experimental set-up. Wild-type (Wt) and *Plin2*$^{-/-}$ bone marrow-derived macrophages (BMDMs) were stimulated with 50 µg/ml myelin for 24h (Lipid droplet (LD) formation) followed by the addition of fresh medium for 24h (LD degradation). **B,C)** Representative images of Oil red O (ORO) (B) and BODIPY (C) staining (n=5-6 wells). Scale bars: 20µm (ORO, B) and 10µm (BODIPY, C). **D,E)** Relative amount of ORO^{+} (D) and BODIPY^{+} (E) LDs (n=3 wells). **F)** Quantification of ORO staining of Wt and *Plin2*$^{-/-}$ BMDMs stimulated with 50µg/ml myelin followed by culture in myelin-free medium for 2, 4, 6, 8 or 24 h (n=3 wells). **G-H)** Free cholesterol (FC) and cholesterol ester (CE) concentration measured using Amplex Red Assay (n=6). **I-J)** Liquid chromatography electrospray ionization tandem mass spectrometry analysis of Wt and *Plin2*$^{-/-}$ BMDMs. Log_2 fold change abundance of all lipid classes is shown (n=4 mice). **K)** Cholesterol efflux capacity of myelin-treated *Plin2*$^{-}$

$^{/-}$ BMDMs normalized to myelin-treated Wt BMDMs (n=10). **L)** Internalization of DiI-labeled myelin (n=8 wells). Data are represented as mean ± SEM. *P ≤ 0.05, **P ≤ 0.01 and ****P ≤ 0.0001.

Plin2-deficient foamy macrophages exhibit a less-inflammatory phenotype

In neurodegenerative disorders, macrophages contribute to CNS lesion progression through the production of inflammatory mediators [31]. As previous studies linked PLIN2 to increased expression of various inflammatory markers [32], we examined the effect of *Plin2*-deficiency on the inflammatory phenotype of control and foamy BMDMs in the presence of the inflammatory cytokines IL1β and IFNγ. *Plin2*-deficiency did not alter mRNA expression levels of inflammatory cytokines and chemokines in control macrophages (Fig. 3A). In contrast, absence of *Plin2* reduced the expression of the pro-inflammatory genes *Tnfa* and *Il6*, and increased the expression of anti-inflammatory *Tgfß* in myelin-containing BMDMs (Fig. 3B,C) . Furthermore, a trend towards a lower production of TNFa and reduced nitric oxide (NO_2^-) levels were measured in the supernatant of *Plin2*$^{-/-}$ myelin-treated macrophages (Fig. 3D,E). Having established that *Plin2*-deficiency enhances LD breakdown (Fig. 2), these findings strongly suggest that PLIN2 drives the phenotype of foamy macrophages to a more inflammatory one by preventing the degradation of LDs.

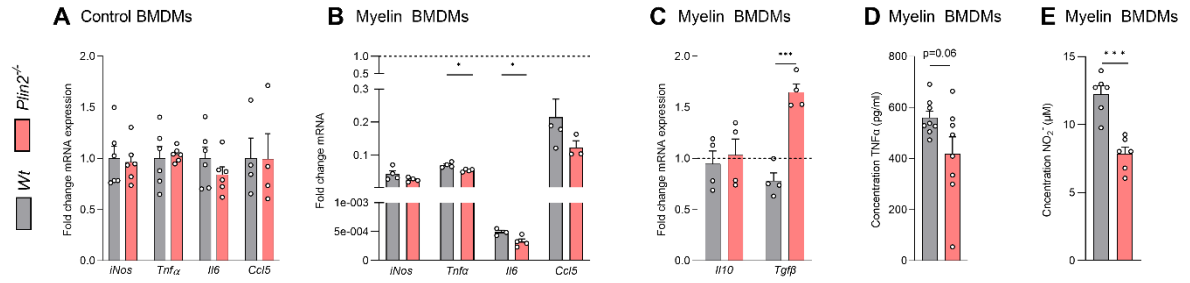

Figure 3. *Plin2*-deficiency in myelin-loaded macrophages reduces the expression of pro-inflammatory mediators. A-C) mRNA expression of pro (A,B)- and anti (C)- inflammatory genes in wild-type (Wt) and *Plin2*$^{-/-}$ bone marrow-derived control (A) and foamy (B,C) macrophages (BMDMs) stimulated with IFNγ and IL1β (both 100 ng/ml) for 6h (n=6 wells). Dotted line represents control Wt and *Plin2*$^{-/-}$ BMDMs stimulated with IFNγ and IL1β. **D,E)** TNFα (D) and NO_2^- (E) concentration in the supernatant of Wt and *Plin2*$^{-/-}$ foamy BMDMs stimulated with IFNγ and IL1β (both 100 ng/ml) for 18h (n=8 wells). Data are represented as mean ± SEM. *P ≤ 0.05, ***P ≤ 0.001.

Plin2-deficiency increases LD degradation by boosting lipolysis

Autophagy is a homeostatic cellular recycling process that mediates the lysosomal delivery and clearance of various cellular components and damaged organelles in double-membraned vesicles termed autophagosomes [33]. A selective form of autophagy called lipophagy targets LDs for

degradation [34]. Accordingly, we recently showed that lipophagy monitors the accumulation and efflux of myelin-derived lipids in macrophages [7]. Based on the latter study and the fact that *Plin2*$^{-/-}$ macrophages showed higher levels of LD degradation and cholesterol efflux, we next aimed to assess whether loss of *Plin2* increases autophagy-mediated turnover of LDs. During lipophagy, the autophagy marker microtubule-associated protein 1A/1B-light chain 3 (LC3) associates with LDs [32]. By using super-resolution Airyscan confocal microscopy, the colocalization of LC3-puncta with LDs was measured in wild-type and *Plin2*$^{-/-}$ myelin-containing macrophages. Interestingly, loss of PLIN2 did not affect the percentage of LC3^{+} LDs (Fig. 4A,C), nor did it affect the general level of LC3-II (Fig. S4). More downstream in the lipophagy pathway, autophagosomes fuse with lysosomes to degrade their cargo. Yet, loss of PLIN2 did not affect the level of colocalization of LAMP1^{+} lysosomes with LDs (Fig. 4B,D). Altogether, these data show that PLIN2 does not reduce LD degradation by protecting LDs from lipophagy-mediated degradation in myelin-containing macrophages.

A second lipid degradation process shown to be responsible for the breakdown of LDs is neutral lipolysis, in which cytosolic adipose triglyceride lipase (ATGL), hormone-sensitive lipase (HSL), and monoacylglycerol lipase (MGL) constitutively cooperate to degrade triacylglycerols into free fatty acids and glycerol. As a result, the amount of free glycerol is proportional to the rate of lipolysis. By measuring intracellular glycerol content, we show that *Plin2*-deficient macrophages have increased lipolysis levels compared to wild-type macrophages, both with and without the addition of myelin (Fig. 4E,F). Accordingly, *Plin2*$^{-/-}$ macrophages showed a higher expression of various cytosolic lipases (Fig. 4G). In conclusion, our results demonstrate that PLIN2 reduces lipolysis-, but not lipophagy-, mediated degradation of LDs.

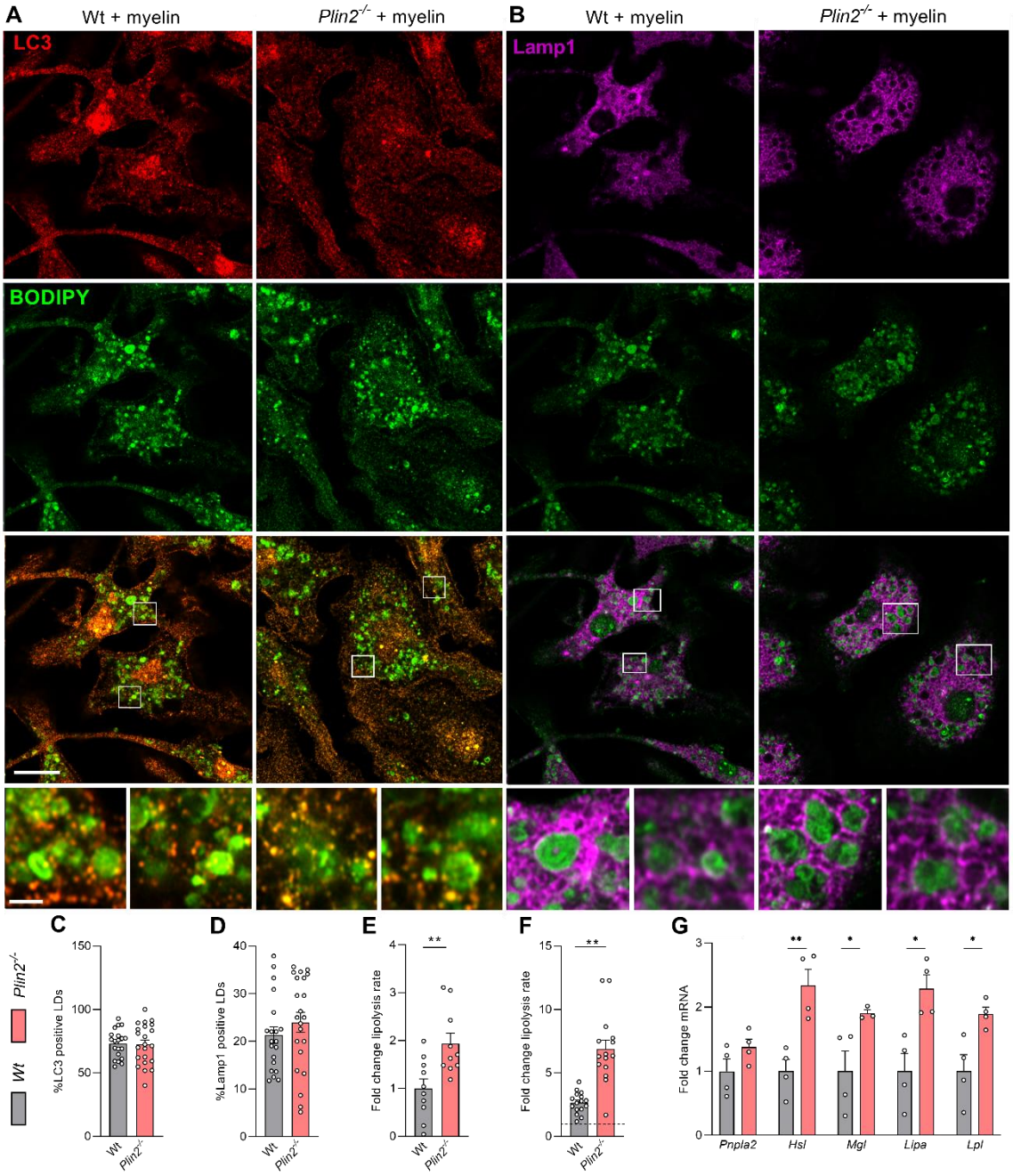

Figure 4. Loss of *Plin2* increases lipolysis in macrophages. A,B) Representative images of immunofluorescence staining of wild-type (Wt) and *Plin2*$^{-/-}$ bone marrow-derived macrophages (BMDMs) treated with 50 µg/ml myelin for 24h. BODIPY (green), LC3 (A, red, n=3 wells), Lamp1 (B, magenta, n=3 wells). Scale bar 10 µm, 2 µm. **C,D)** Average percentage of (C) LC3^{+} and (D) Lamp1^{+} lipid droplets (LDs) of the total amount of LDs. **E,F)** Glycerol concentration was measured in Wt and *Plin2*$^{-/-}$ (E) control and (F) foamy BMDMs cultured in the presence of myelin-free medium for 24h. Results are normalized for the amount of LDs and compared to untreated genotype controls (F, dotted line, n=3 wells). **(G)** mRNA expression of lipase genes in Wt and *Plin2*$^{-/-}$ BMDMs (n=4 wells). All data are represented as mean ± SEM. *P<0.05; **P< 0.01.

Loss of PLIN2 improves remyelination in an ex vivo cerebellar brain slice model

We and others demonstrated that the intracellular accumulation of myelin-derived lipids drives macrophages towards an inflammatory phenotype that suppresses CNS repair [5-7]. Given that our results show that PLIN2 boosts foam cell formation by reducing LD degradation, we next aimed to assess whether absence of PLIN2 promotes remyelination. To this end, we used the *ex vivo* cerebellar brain slice model in which lysolecithin-induced demyelination is followed by endogenous remyelination (Fig. S5A). Akin to our *in vitro* findings, *Plin2*-deficiency reduced the accumulation of LDs in remyelinating brain slices (Fig. 5A,B). Reduced LD levels were accompanied by increased glycerol levels in the brain slice medium, pointing towards increased levels of lipolysis and lipid efflux in *Plin2*$^{-/-}$ brain slices (Fig. 5C). Furthermore, a lower inflammatory gene expression was detected in *Plin2*-deficient slices (Fig. 5D). Importantly, *Plin2*$^{-/-}$ brain slices showed enhanced levels of remyelination, measured by analysing the colocalization of myelin basic protein (myelin marker, MBP) and neurofilament (axonal marker, NF) (Fig. 5E,F). Three-dimensional reconstruction of cerebellar slices confirmed more efficient remyelination (Fig. 5E,F). To elucidate the role of microglia in this observed beneficial effect on remyelination, we used brain slice cultures in which microglia were depleted using clodronate liposomes prior to demyelination (Fig. S5A). The efficacy of depletion was confirmed using F4/80 staining of brain slices treated with empty control liposomes and clodronate liposomes (Fig. S5B,C). In the absence of microglia, the protective effect of *Plin2*$^{-/-}$ on remyelination was abolished, confirming that loss of *Plin2* boosts remyelination in a microglia-dependent manner (Fig. 5E,G). Of note, loss of *Plin2* did not affect the differentiation of oligodendrocyte precursor cells (OPCs) towards mature oligodendrocytes (Fig. S5D,E). In conclusion, these findings demonstrate that *Plin2*-deficiency increases lipolysis-mediated LD degradation in phagocytes, thereby reducing inflammation and improving remyelination *ex vivo*.

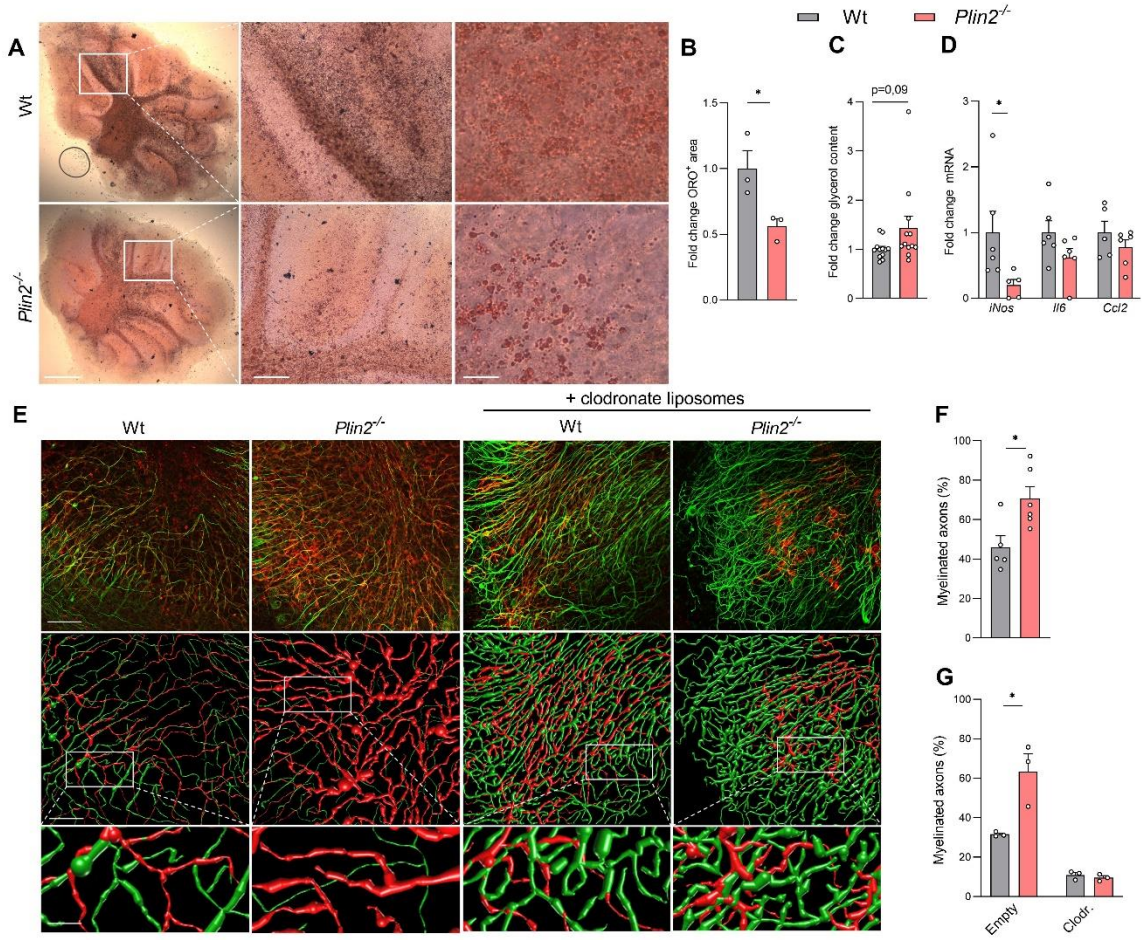

Figure 5. Loss of *Plin2* improves remyelination in *ex vivo* brain slice cultures. A,B) Representative images and quantification of Oil Red O (ORO) staining of cerebellar brain slices (n=3 slices). Scale bars 500 µm, 100 µm, 50 µm. **C)** Relative glycerol concentration measured in supernatant of the brain slice cultures during remyelination (n=6 wells). **D)** mRNA expression of *iNos*, *Il6*, and *Ccl2* in brain slices during remyelination (n=6 slices). **E)** Representative immunofluorescence images (top) and three-dimensional reconstructions (bottom) of brain slices stimulated with or without clodronate liposomes (0.5 mg/ml). Scale bars 150 µm, 150 µm, 50µm. **F,G)** MBP^+NF^+ axons of total NF^+ axons in wild-type and *Plin2*$^{-/-}$ slices stimulated with empty or clodronate (Clodr.) liposomes (G), or unstimulated (F) (n=3-6 slices). All data are represented as mean ± SEM. *P< 0.05.

Plin2-deficiency improves remyelination after cuprizone-induced demyelination in vivo

To validate the significance of our findings *in vivo*, we used the cuprizone-induced de- and remyelination model. Cuprizone feeding leads to demyelination in the corpus callosum and cessation of cuprizone administration after 6 weeks causes spontaneous remyelination. Animals were pathologically characterized both after demyelination (6 weeks, 6w) and during spontaneous remyelination (7 weeks, 7w) (Fig. S6A). We confirm our *in vitro* and *ex vivo* findings and show that loss of *Plin2* reduced the amount of ORO^+ LDs during remyelination after correction for the number

of F4/80^{+} phagocytes in the corpus callosum (Fig. 6A,C,D,F). Furthermore, iNOS presence was lower in *Plin2*$^{-/-}$ animals during demyelination (Fig. 6B,E), and there was a reduced expression of inflammatory genes *Ccl4*, *Il6* and *Tnfa* measured in the corpus callosum during de- and remyelination (Fig. 6G,H). Importantly, *Plin2*$^{-/-}$ mice showed an increased MBP immunoreactivity during remyelination (Fig. 6I,J), without showing changes in the presence of degenerated myelin (Fig. S6B,C). Finally, akin to our *in vitro* findings, *Plin2*-deficiency resulted in a higher gene expression of *Atgl* and *Mgl*, suggesting that a higher rate of lipolysis-mediated LD degradation lies at the base of the lower lipid load (Fig. 6K). Collectively, our results show that *Plin2*-deficiency reduces macrophage LD load and inflammation *in vivo*, and enhances remyelination. In conclusion, we identify PLIN2 as a novel therapeutic target to promote remyelination.

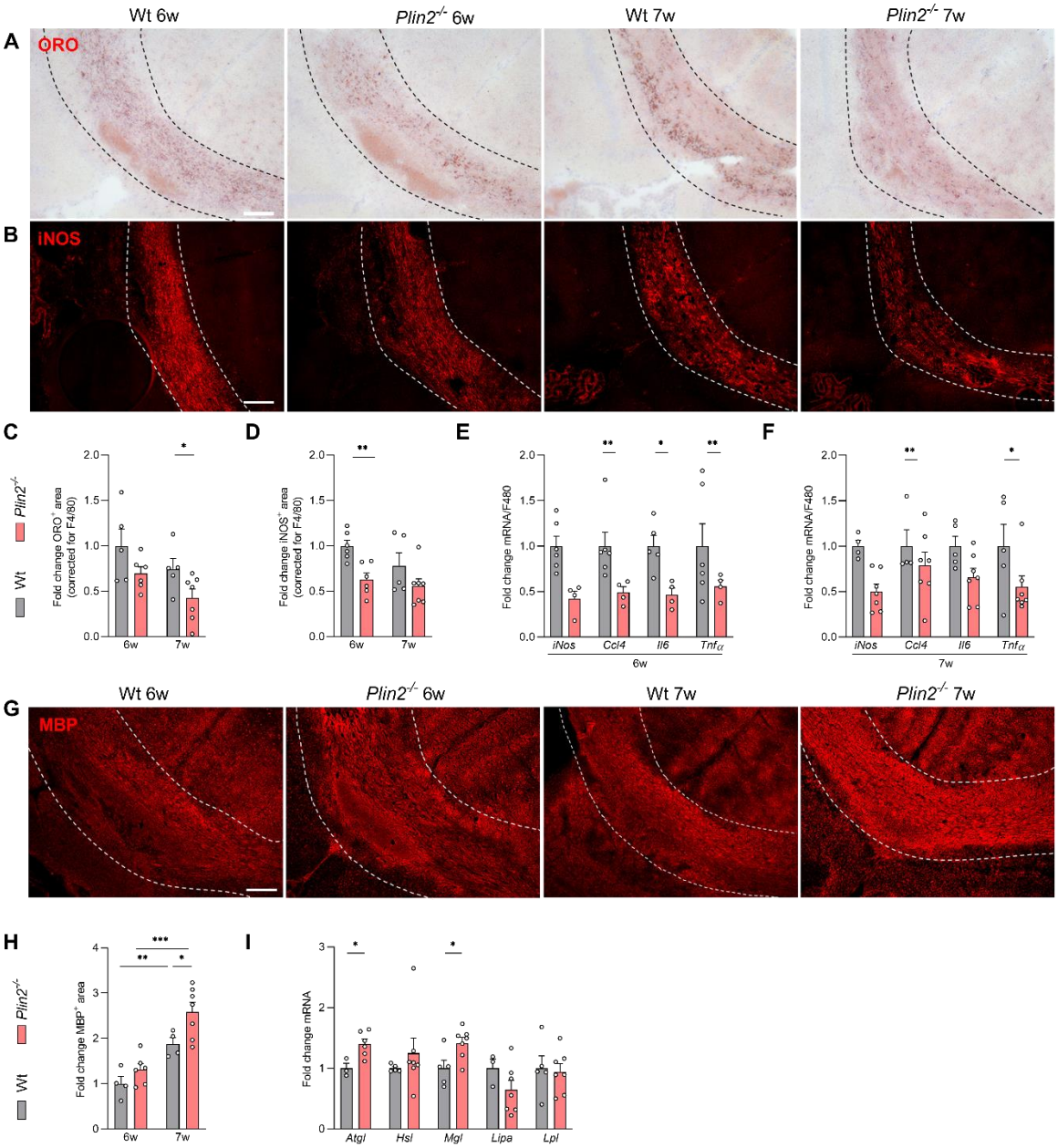

Figure 6. *Plin2*-deficiency stimulates remyelination in the cuprizone model. Wild-type (Wt) and *Plin2*$^{-/-}$ mice were fed a cuprizone diet for 6 weeks to induce demyelination in the corpus callosum (CC). Upon withdrawal of the cuprizone diet, spontaneous remyelination ensues. Tissue was collected after demyelination (6w) and after 1 week of recovery (7w). **A-F)** Representative images and quantification of Oil Red O (ORO) (A,D), immunofluorescence iNOS (B,E), and F4/80 (C,F) staining of the CC (scale bar 100 µm, n=4-7 mice). **G-H)** mRNA expression of inflammatory mediators in the CC (n=4-6 mice). **I,J)** Representative images (I) and quantification (J) of myelin basic protein (MBP) staining of the CC (scale bar 100µm, n=4-7 mice). **K)** mRNA expression of lipase genes in the CC during remyelination (n=3-7 mice). All data are represented as mean ± SEM. *P< 0.05; **P<0.01; ***P<0.001.

DISCUSSION

Foamy phagocytes containing excessive amounts of LDs are a pathological hallmark of demyelinating disorders affecting the CNS [1, 5]. However, to date, the impact of LDs on foamy macrophage and microglia physiology and lesion progression, as well as the molecular mechanisms involved in LD biogenesis and breakdown, remain poorly understood. Here, we provide evidence for a key role of the main LD-associated protein PLIN2 in the regulation of LD degradation in foamy macrophages. We show that myelin uptake strongly increases PLIN2 in a PPARγ-dependent manner. Loss of *Plin2* reduced LD accumulation by boosting lipolysis-mediated degradation, directed foam cells towards a less inflammatory functional phenotype, and markedly improved remyelination in the *ex vivo* brain slice model and the *in vivo* cuprizone-induced demyelination model.

We demonstrate that foamy phagocytes in actively demyelinating MS lesions show a marked increased PLIN2 abundance as compared to phagocytes in the surrounding NAWM. Accordingly, *Plin2* expression was highly increased in the CNS of experimental models for autoimmune- and toxin-induced demyelination [23, 35], as well as in *in vitro* cultures mimicking the formation of myelin-containing macrophages. Consistent with these findings, other studies demonstrated that PLIN2 levels are increased in macrophages exposed to lipid ligands such as modified low-density lipoproteins (LDL) [16, 18, 36, 37], indicating that PLIN2 expression is generally increased by lipid uptake. Furthermore, foamy hepatocytes in animals fed a high-fat diet show elevated PLIN2 levels on LDs [38, 39]. We further provide evidence that PPARγ, a ligand-dependent transcription factor known to regulate various aspects of cellular lipid metabolism, partially controls *Plin2* expression in myelin-containing macrophages. In line with these findings, previous studies defined that PPARγ regulates the transcription of *Plin2* by binding to the PPAR response element present in the *Plin2* gene [25-27]. Moreover, we recently demonstrated that myelin-containing macrophages show active PPAR signalling *in vitro* and in demyelinating MS lesions [4, 24]. Collectively, these findings indicate that myelin-induced PPARγ-signalling increases PLIN2 expression in macrophages.

Previous studies demonstrated that PLIN2 controls LD metabolism, thereby having a major impact on LD load, cellular fitness, and disease. Here, we show that PLIN2 regulates LD metabolism in myelin-laden macrophages by inhibiting LD degradation and lipid efflux. Accordingly, *Plin2* overexpression was previously found to increase cellular LD load and impair lipid efflux in oxidized LDL-treated macrophages [18]. Similar, increased PLIN2 abundance in trophoblasts is linked to enhanced accumulation of LDs, hypoxia, and apoptotic cell death [40]. Next to LD breakdown, cellular

changes in LD load can be a result of alterations in LD biogenesis [1]. Yet, we found no differences in LD formation in *Plin2*-deficient myelin-laden macrophages. In contrast, previous studies showed that overexpression of *Plin2* increases LD accumulation by stimulating triacylglycerol synthesis in VLDL-treated macrophages [18, 41]. Furthermore, *Plin2*-deficiency was found to impair macrophage LD formation and protect against atherosclerosis [16]. More research is warranted to unravel why PLIN2 does not impact LD biogenesis in myelin-containing macrophages. Given that cholesterol is a major lipid constituent of myelin, our findings might merely reflect changes in lipid ligands and thus LD lipid constituents. On the other hand, as cholesterol is predominantly present in its free form in myelin [42], PLIN2 might not affect cholesterol esterification and LD biogenesis to protect myelin-containing macrophages against free cholesterol-induced lipotoxicity [8]. With respect to the latter, defective LD biogenesis was recently found to impair the regenerative response after demyelination through induction of endoplasmic reticulum stress [43]. Consistent with a protective function of PLIN2 in myelin-containing macrophages, we did not detect changes in cell viability in myelin-laden *Plin2*$^{-/-}$ macrophages. Notably, next to a lower presence of cholesterol and tri- and diacylglycerides, loss of *Plin2* also caused alterations in other lipid species. For instance, *Plin2*$^{-/-}$ macrophages showed a prominent reduction in lysophosphatidylcholine (LPC) and lysophosphatidylethanolamine (LPE) during LD formation and degradation. Interestingly, LPC is believed to play an important role in inflammatory diseases by stimulating pro-inflammatory signal transduction and cytokine expression in macrophages and other cell types [44], which is in line with the less inflammatory phenotype which *Plin2*$^{-/-}$ BMDMs display. Furthermore, multiple phospholipid classes were present to a smaller extent in *Plin2*$^{-/-}$ macrophages during LD degradation. As phospholipids make up the monolayer barrier between LDs and the cytosol, this decrease is in line with a decreased presence of LDs in *Plin2*$^{-/-}$ BMDMs. Collectively, our findings show that PLIN2 protects myelin-derived LDs from degradation in macrophages, without affecting LD biogenesis, resultingly boosting foam cell formation.

Recently, we demonstrated that lipophagy, which entails autophagosomal degradation of LDs, controls LD breakdown in myelin-containing macrophages [7]. Despite PLIN2 affecting lipophagy-mediated degradation of LDs in macrophages, hepatocytes, and cardiomyocytes [45-48], we here show that loss of PLIN2 does not change the level of lipophagy in myelin-containing macrophages. Instead, our findings indicate that PLIN2 controls LD degradation through lipolysis. Neutral lipolysis involves cytoplasmic lipases [49], such as PNPLA2/ATGL (patatin-like phospholipase domain

containing 2), that promote triacylglycerol hydrolysis and the release of glycerol and free fatty acids [18]. Accordingly, our results show that *Plin2*-deficient control and foamy macrophages show increased release of free glycerol, indicative of increased lipolysis, which was accompanied by a higher expression of multiple lipases including *Pnpla2*. Of interest, PLIN2 expression has previously been linked to reduced lipolysis-mediated LD turnover by decreasing the affinity of ATGL to LDs [50, 51]. In summary, our results indicate that in agreement with other cell types, absence of PLIN2 makes LDs in myelin-laden macrophages more prone for lipolysis-mediated degradation.

In demyelinating disorders, foamy phagocytes accumulate large amount of lipids and cytosolic LDs, and display an inflammatory, repair-suppressive phenotype [5, 7]. Here, we show that *Plin2*-deficiency boosts LD degradation in foamy macrophages *in vitro*, and, in parallel, reduces the expression of inflammatory and toxic mediators. These data suggest that PLIN2 represents an interesting therapeutic target to reduce neuroinflammation in demyelinating disorders. Notably, while previous studies found that overexpression of *Plin2* in macrophages induces the expression of *Tnfa* and *Il6* [32], *Plin2*-deficiency did not alter the inflammatory transcriptional profile of control macrophages in our experiments. Consistent with the importance of inflammation in suppressing CNS repair, we further provide evidence that loss of *Plin2* improves remyelination in an *ex vivo* cerebellar brain slice model and in the *in vivo* cuprizone model. Similar to our *in vitro* findings, *Plin2*-deficiency resulted in increased lipolysis-mediated LD degradation and a reduced inflammatory burden during remyelination. It remains unclear why PLIN2 expression remains elevated in lesional foamy phagocytes as its expression is associated with reduced CNS repair. Faulty feedback regulation might explain incessant high expression levels of PLIN2 in phagocytes in MS lesions. In atherosclerotic lesions, uptake of modified LDL by macrophages was found to activate PPARγ, resulting in elevated expression of the PPARγ response gene *Cd36* and additional CD36-mediated LDL uptake [52, 53]. As PPARγ is a main regulator of PLIN2 expression in foamy macrophages, this feedforward regulation may explain high PLIN2 abundance in foamy phagocytes in MS lesions. Interestingly, we previously showed that oxidized forms of myelin divergently impact foamy phagocyte physiology. While uptake of oxidized myelin leads to an uncontrolled increase in the scavenger receptor collection placenta 1 (CL-P1), the initial increase in CL-P1 expression upon uptake of unmodified myelin rapidly subsides [54]. Hence, the formation and uptake of modified forms of myelin in MS lesions could explain high lesional PLIN2 levels.

It is important to note that precaution should be taken when targeting PLIN2 in future remyelinating therapies, as LDs have important protective functions as well [55]. First, the storage of excess free fatty acids and cholesterol in LDs is essential to prevent cells from lipid-induced cytotoxicity, and serves as a reservoir of energy for the cell [56, 57]. Furthermore, LDs form connections with mitochondria and the ER and can modulate mitochondria bioenergetics and the ER-stress response [58]. In addition, cholesterol, which is the main component of myelin-derived LDs, is an important activator of anti-inflammatory signalling pathways [3, 59, 60]. Finally, Gouna et al. recently demonstrated that LD formation is crucial to allow efficient lesion recovery *in vivo* [43]. Given that we found that PLIN2 controls LD degradation and not formation, this study can explain why *Plin2* does not reduce cellular viability and boosts disease-resolving characteristics in myelin-containing macrophages. All in all, our findings show that that reducing PLIN2 expression is a promising therapeutic strategy to reduce foam cell formation and induce remyelination.

In summary, we demonstrate an increased expression of PLIN2 in foamy macrophages in MS in a PPARγ-dependent manner. *Plin2*-deficiency was able to boost LD turnover and skew myelin-containing macrophages towards a less inflammatory, reparative phenotype. In conclusion, we provide evidence for PLIN2 to serve as a bridge between LD overload and demyelinating disorders, and identify it as an interesting target for future reparative therapies for MS.

STATEMENTS AND DECLARATIONS

Funding

The work has been supported by the Flemish Fund for Scientific Research (FWO Vlaanderen; 1141920N, 1S15519N), and the special research fund UHasselt (BOF).

Competing interests

The authors declare no competing interests exist.

Author contributions

M. Loix, E. Wouters, M. Haidar, J.F.J. Bogie, and J.J.A. Hendriks conceived experiments. M. Loix, E. Wouters, S. Vanherle, J. Dehairs, and M. Haidar performed experiments. M. Loix, E. Wouters, S. Vanherle, J. Dehairs and M. Haidar analysed data. M. Loix, E. Wouters, S. Vanherle, H. Kemps, M. Haidar, J.F.J. Bogie, and J.J.A. Hendriks discussed results. J.L. McManaman provided the animals. M. Loix, E. Wouters, and J.F.J. Bogie wrote the manuscript. All authors have read and approved the manuscript.

Data availability

The datasets generated during and/or analysed during the current study are not publicly available but are available from the corresponding author on reasonable request.

Ethics statement

Animal experiments in this study were carried out in accordance with the recommendations of the institutional animal care and use committee of Hasselt University. The protocol was approved by the institutional animal care and use committee of Hasselt University (protocol numbers: 201840, 201920, 201953).

ACKNOWLEDGEMENTS

We thank M.P. Tulleners and L. Timmermans for excellent technical assistance.

References

1. Grajchen, E., J.J.A. Hendriks, and J.F.J. Bogie, *The physiology of foamy phagocytes in multiple sclerosis.* Acta Neuropathol Commun, 2018. **6**(1): p. 124.
2. Bogie, J., et al., *Myelin-phagocytosing macrophages modulate autoreactive T cell proliferation.* Journal of Neuroinflammation, 2011. **8**(1): p. 85.
3. Bogie, J.F., et al., *Myelin-derived lipids modulate macrophage activity by liver X receptor activation.* PLoS One, 2012. **7**(9): p. e44998.
4. Bogie, J.F., et al., *Myelin alters the inflammatory phenotype of macrophages by activating PPARs.* Acta Neuropathol Commun, 2013. **1**: p. 43.
5. Bogie, J.F.J., et al., *Stearoyl-CoA desaturase-1 impairs the reparative properties of macrophages and microglia in the brain.* J Exp Med, 2020. **217**(5).
6. Cantuti-Castelvetri, L., et al., *Defective cholesterol clearance limits remyelination in the aged central nervous system.* Science, 2018. **359**(6376): p. 684-688.
7. Haidar, M., et al., *Targeting lipophagy in macrophages improves repair in multiple sclerosis.* Autophagy, 2022: p. 1-14.
8. Olzmann, J.A. and P. Carvalho, *Dynamics and functions of lipid droplets.* Nat Rev Mol Cell Biol, 2019. **20**(3): p. 137-155.
9. Plakkal Ayyappan, J., A. Paul, and Y.H. Goo, *Lipid droplet-associated proteins in atherosclerosis (Review).* Mol Med Rep, 2016. **13**(6): p. 4527-34.
10. Walther, T.C., J. Chung, and R.V. Farese, Jr., *Lipid Droplet Biogenesis.* Annu Rev Cell Dev Biol, 2017. **33**: p. 491-510.
11. Shiffman, D., et al., *Large scale gene expression analysis of cholesterol-loaded macrophages.* J Biol Chem, 2000. **275**(48): p. 37324-32.
12. Bickel, P.E., J.T. Tansey, and M.A. Welte, *PAT proteins, an ancient family of lipid droplet proteins that regulate cellular lipid stores.* Biochimica Et Biophysica Acta-Molecular and Cell Biology of Lipids, 2009. **1791**(6): p. 419-440.
13. Buechler, C., et al., *Adipophilin is a sensitive marker for lipid loading in human blood monocytes.* Biochim Biophys Acta, 2001. **1532**(1-2): p. 97-104.
14. Imamura, M., et al., *ADRP stimulates lipid accumulation and lipid droplet formation in murine fibroblasts.* Am J Physiol Endocrinol Metab, 2002. **283**(4): p. E775-83.
15. Xu, S., et al., *Perilipin 2 and lipid droplets provide reciprocal stabilization.* Biophysics Reports, 2019. **5**(3): p. 145-160.
16. Paul, A., et al., *Deficiency of adipose differentiation-related protein impairs foam cell formation and protects against atherosclerosis.* Circ Res, 2008. **102**(12): p. 1492-501.
17. Larigauderie, G., et al., *Adipophilin increases triglyceride storage in human macrophages by stimulation of biosynthesis and inhibition of beta-oxidation.* FEBS J, 2006. **273**(15): p. 3498-510.
18. Larigauderie, G., et al., *Adipophilin enhances lipid accumulation and prevents lipid efflux from THP-1 macrophages: potential role in atherogenesis.* Arterioscler Thromb Vasc Biol, 2004. **24**(3): p. 504-10.
19. McManaman, J.L., et al., *Perilipin-2-null mice are protected against diet-induced obesity, adipose inflammation, and fatty liver disease.* J Lipid Res, 2013. **54**(5): p. 1346-59.
20. Erwig, M.S., et al., *Myelin: Methods for Purification and Proteome Analysis.* Methods Mol Biol, 2019. **1936**: p. 37-63.
21. Jorissen, W., et al., *Relapsing-remitting multiple sclerosis patients display an altered lipoprotein profile with dysfunctional HDL.* Sci Rep, 2017. **7**: p. 43410.
22. Fan, B., et al., *High glucose, insulin and free fatty acid concentrations synergistically enhance perilipin 3 expression and lipid accumulation in macrophages.* Metabolism, 2013. **62**(8): p. 1168-79.
23. Grajchen, E., et al., *CD36-mediated uptake of myelin debris by macrophages and microglia reduces neuroinflammation.* J Neuroinflammation, 2020. **17**(1): p. 224.

24. Wouters, E., et al., *Altered PPARγ Expression Promotes Myelin-Induced Foam Cell Formation in Macrophages in Multiple Sclerosis.* International journal of molecular sciences, 2020. **21**(23): p. 9329.
25. Bildirici, I., et al., *The lipid droplet-associated protein adipophilin is expressed in human trophoblasts and is regulated by peroxisomal proliferator-activated receptor-gamma/retinoid X receptor.* J Clin Endocrinol Metab, 2003. **88**(12): p. 6056-62.
26. Schadinger, S.E., et al., *PPARgamma2 regulates lipogenesis and lipid accumulation in steatotic hepatocytes.* Am J Physiol Endocrinol Metab, 2005. **288**(6): p. E1195-205.
27. Targett-Adams, P., et al., *A PPAR response element regulates transcription of the gene for human adipose differentiation-related protein.* Biochim Biophys Acta, 2005. **1728**(1-2): p. 95-104.
28. Bickel, P.E., J.T. Tansey, and M.A. Welte, *PAT proteins, an ancient family of lipid droplet proteins that regulate cellular lipid stores.* Biochim Biophys Acta, 2009. **1791**(6): p. 419-40.
29. Kimmel, A.R., et al., *Adoption of PERILIPIN as a unifying nomenclature for the mammalian PAT-family of intracellular lipid storage droplet proteins.* J Lipid Res, 2010. **51**(3): p. 468-71.
30. Fukushima, M., et al., *Adipose differentiation related protein induces lipid accumulation and lipid droplet formation in hepatic stellate cells.* In Vitro Cellular & Developmental Biology - Animal, 2005. **41**(10): p. 321-324.
31. Bogie, J.F., P. Stinissen, and J.J. Hendriks, *Macrophage subsets and microglia in multiple sclerosis.* Acta Neuropathol, 2014. **128**(2): p. 191-213.
32. Chen, F.L., et al., *Adipophilin affects the expression of TNF-alpha, MCP-1, and IL-6 in THP-1 macrophages.* Mol Cell Biochem, 2010. **337**(1-2): p. 193-9.
33. Klionsky, D.J., et al., *Guidelines for the use and interpretation of assays for monitoring autophagy (3rd edition).* Autophagy, 2016. **12**(1): p. 1-222.
34. Singh, R., et al., *Autophagy regulates lipid metabolism.* Nature, 2009. **458**(7242): p. 1131-1135.
35. Lampron, A., et al., *Inefficient clearance of myelin debris by microglia impairs remyelinating processes.* J Exp Med, 2015. **212**(4): p. 481-95.
36. Becker, L., et al., *A macrophage sterol-responsive network linked to atherogenesis.* Cell Metab, 2010. **11**(2): p. 125-35.
37. Son, S.H., et al., *Perilipin 2 (PLIN2)-deficiency does not increase cholesterol-induced toxicity in macrophages.* PLoS One, 2012. **7**(3): p. e33063.
38. Nocetti, D., et al., *Lipid droplets are both highly oxidized and Plin2-covered in hepatocytes of diet-induced obese mice.* Appl Physiol Nutr Metab, 2020. **45**(12): p. 1368-1376.
39. Crunk, A.E., et al., *Dynamic regulation of hepatic lipid droplet properties by diet.* PLoS One, 2013. **8**(7): p. e67631.
40. Bildirici, I., et al., *PLIN2 Is Essential for Trophoblastic Lipid Droplet Accumulation and Cell Survival During Hypoxia.* Endocrinology, 2018. **159**(12): p. 3937-3949.
41. Larigauderie, G., et al., *Adipophilin increases triglyceride storage in human macrophages by stimulation of biosynthesis and inhibition of beta-oxidation.* Febs j, 2006. **273**(15): p. 3498-510.
42. Saher, G. and S.K. Stumpf, *Cholesterol in myelin biogenesis and hypomyelinating disorders.* Biochim Biophys Acta, 2015. **1851**(8): p. 1083-94.
43. Gouna, G., et al., *TREM2-dependent lipid droplet biogenesis in phagocytes is required for remyelination.* J Exp Med, 2021. **218**(10).
44. Matsumoto, T., T. Kobayashi, and K. Kamata, *Role of lysophosphatidylcholine (LPC) in atherosclerosis.* Curr Med Chem, 2007. **14**(30): p. 3209-20.
45. Mardani, I., et al., *Plin2-deficiency reduces lipophagy and results in increased lipid accumulation in the heart.* Sci Rep, 2019. **9**(1): p. 6909.
46. Tsai, T.H., et al., *The constitutive lipid droplet protein PLIN2 regulates autophagy in liver.* Autophagy, 2017. **13**(7): p. 1130-1144.
47. Saliba-Gustafsson, P., et al., *Subclinical atherosclerosis and its progression are modulated by PLIN2 through a feed-forward loop between LXR and autophagy.* J Intern Med, 2019. **286**(6): p. 660-675.

48. Feng, X., et al., *Autophagy involved in lipopolysaccharide-induced foam cell formation is mediated by adipose differentiation-related protein.* Lipids Health Dis, 2014. **13**: p. 10.
49. Zechner, R., F. Madeo, and D. Kratky, *Cytosolic lipolysis and lipophagy: two sides of the same coin.* Nat Rev Mol Cell Biol, 2017. **18**(11): p. 671-684.
50. Listenberger, L.L., et al., *Adipocyte differentiation-related protein reduces the lipid droplet association of adipose triglyceride lipase and slows triacylglycerol turnover.* J Lipid Res, 2007. **48**(12): p. 2751-61.
51. Russell, T.D., et al., *Adipophilin regulates maturation of cytoplasmic lipid droplets and alveolae in differentiating mammary glands.* J Cell Sci, 2011. **124**(Pt 19): p. 3247-53.
52. Ishii, T., et al., *Role of Nrf2 in the regulation of CD36 and stress protein expression in murine macrophages: activation by oxidatively modified LDL and 4-hydroxynonenal.* Circ Res, 2004. **94**(5): p. 609-16.
53. Nagy, L., et al., *Oxidized LDL regulates macrophage gene expression through ligand activation of PPARgamma.* Cell, 1998. **93**(2): p. 229-40.
54. Bogie, J.F., et al., *Scavenger receptor collectin placenta 1 is a novel receptor involved in the uptake of myelin by phagocytes.* Sci Rep, 2017. **7**: p. 44794.
55. Haidar, M., et al., *Lipophagy: a new player in CNS disorders.* Trends Endocrinol Metab, 2021. **32**(11): p. 941-951.
56. Cingolani, F. and M.J. Czaja, *Regulation and Functions of Autophagic Lipolysis.* Trends in Endocrinology & Metabolism, 2016. **27**(10): p. 696-705.
57. Ouimet, M. and Y.L. Marcel, *Regulation of Lipid Droplet Cholesterol Efflux From Macrophage Foam Cells.* Arteriosclerosis, Thrombosis, and Vascular Biology, 2012. **32**(3): p. 575-581.
58. Cohen, S., *Chapter Three - Lipid Droplets as Organelles*, in *International Review of Cell and Molecular Biology*, L. Galluzzi, Editor. 2018, Academic Press. p. 83-110.
59. Boven, L.A., et al., *Myelin-laden macrophages are anti-inflammatory, consistent with foam cells in multiple sclerosis.* Brain, 2006. **129**(Pt 2): p. 517-26.
60. Hikawa, N. and T. Takenaka, *Myelin-stimulated macrophages release neurotrophic factors for adult dorsal root ganglion neurons in culture.* Cell Mol Neurobiol, 1996. **16**(4): p. 517-28.